PHOTONICS Research

Superior third-order nonlinearity in inorganic fullerene-like WS_2 nanoparticles

Tianlun Li,[1,†] Rui Hao,[1,†] Lingling Zhang,[1] Jianyong Mao,[1] Feng Li,[1] Yanpeng Zhang,[1] Jixiang Fang,[1,2] and Lei Zhang[1,*]

[1]Key Laboratory for Physical Electronics and Devices of the Ministry of Education & Shaanxi Key Laboratory of Information Photonic Technique, School of Electronic Science and Engineering, Xi'an Jiaotong University, Xi'an 710049, China
[2]e-mail: jxfang@mail.xjtu.edu.cn
*Corresponding author: eiezhanglei@xjtu.edu.cn

Received 3 June 2020; revised 15 September 2020; accepted 27 September 2020; posted 28 September 2020 (Doc. ID 399490); published 20 November 2020

Two-dimensional (2D) transition metal dichalcogenides (TMDs) attain increasing attention due to their exceptional nonlinear optical efficiencies, which hold promising potential for on-chip photonics and advanced optoelectronic applications. Planar TMDs have been proven to support orders-higher third-order nonlinear coefficients in comparison with common nonlinear materials. Interestingly, stronger light–matter interaction could be motivated when curved features are introduced to 2D TMDs. Here, a type of inorganic fullerene-like WS_2 nanoparticles is chemically synthesized using hard mesoporous silica. By using the spatial self-phase modulation (SSPM) method, the nonlinear refractive index n_2 and third-order susceptibility $\chi^{(3)}$ are investigated in the visible range. It is found that $n_2 \sim 10^{-5}$ cm^2/W and $\chi^{(3)} \sim 10^{-7}$ esu, two orders higher than the counterparts of planar WS_2 structures. Our experimental findings provide a fresh thinking in designing nonlinear optical materials and endow TMDs with new potentials in photonic integration applications.

https://doi.org/10.1364/PRJ.399490

1. INTRODUCTION

Nonlinear optical effects ignite exciting light–matter interactions and greatly enlarge optical applications such as frequency conversion, optical imaging, and information processing [1,2]. Remarkable achievements have been made based on novel working principles [3] and materials [4,5] and their marriage [6–8]. However, one of the main challenges hindering the full exploration of nonlinear effects is the low intrinsic nonlinear susceptibilities of conventional materials. Over the past decade, two-dimensional (2D) materials have attracted increasing attention due to their outstanding optical, electronic, and mechanical properties [9–12]. As a typical example, transition metal dichalcogenides (TMDs) possess layer-dependent electronic bandstructure and thus tunable linear and nonlinear optical properties [13,14]. In particular, third-order nonlinearity holds unique importance for applications in mode-locked lasers, sensors [15], and all-optical switching and modulation [16]. To characterize the third-order susceptibility, various methods have been proposed, such as Z-scan [17,18], four-wave mixing [19], and spatial self-phase modulation (SSPM) [20].

So far, the exploration of optical properties of TMD materials has been mainly focused on various flat 2D structures, including nanosheets or nanoflakes [21–23]. However, in addition to the size, shape, thickness, and material quality of TMDs, the geometric characteristics are also supposed to greatly affect their optical properties [24]. In contrast, inorganic fullerene-like (IF-like) 2D nanoparticles (NPs) with curved geometric features introduce an additional freedom to control and enhance the light–matter interaction strength [25,26]. Initially, they are widely investigated as an efficient lubrication material [27,28]. Recently, it was found that the curved features are prone to symmetry breaking to 2D materials and then making the silent phonon mode Raman active [26,29,30]. It is thus naturally speculated that other nonlinear effects may be enhanced with the curved features.

Here, IF-like WS_2 NPs are chemically synthesized using hard mesoporous silica. The nonlinear refractive index n_2 and third-order susceptibility $\chi^{(3)}$ are characterized using the SSPM method in the visible range. It is found that the nonlinear optical responses of the proposed structures are orders stronger than the counterparts of planar 2D WS_2 films. Therefore, we believe that curved 2D materials could play a growing role in designing optical materials with superior efficiencies at each order of nonlinearity and are endowed with new potentials in high-speed optical signal processes and photonic integration applications.

2327-9125/20/121881-07 Journal © 2020 Chinese Laser Press

2. EXPERIMENT

The IF-like WS_2 NPs are chemically synthesized using ordered three-dimensional (3D) mesoporous silica (EP-FDU-12) as hard templates. The average diameter of the pores and thickness of the wall are 27 nm and 5 nm, respectively. The precursor, i.e., phosphotungstic acid (PTA), is incorporated into the template via a solvent evaporation process. The WS_2 NPs can then be obtained by removing the template in H_2S gas. A typical scanning electron microscopy (SEM, JEOL, JSM-7000F) image of the synthesized WS_2 NPs is shown in Fig. 1(a). The multilayer structure with an interlayer distance of ~0.67 nm is clearly characterized using a high-resolution transmission electron microscopy (HRTEM, JEOL, JEM-2100F) image [Fig. 1(b)]. The synthesized WS_2 NPs hold IF-like features with an average diameter of ~26.5 nm, which do not exhibit a quantum size effect [25]. It is obvious that the NPs show curved multilayered features with a layer number >5 [Fig. 1(b)]. The peaks in the X-ray diffraction (XRD, Bruker, D8 Advance) pattern match well with the standard WS_2 structure (JCPDS card No: 08-0237) [Fig. 1(c)].

Two Raman peaks are observed at ~353 and ~420 cm^{-1} under the excitations of 532 and 633 nm continuous-wave (CW) lasers [Fig. 1(d)]. The Raman active lattice vibrations at the Γ point of the hexagonal Brillion zone are modes 421 cm^{-1} and 356 cm^{-1} in the detected region [31,32]. Furthermore, second-order Raman transition, i.e., two longitudinal acoustic (2LA) phonons at ~353 cm^{-1}, are also observed for excitation energies close to the band gap. More interesting is the activation of the B_{1u} mode, which is silent in planar 2D TMDs. Its excitation arises from the curved layers and structural disorder of WS_2 NPs [26,29,30].

Under the illumination of an incoherent white light source, the transmittance was obtained by normalizing the transmitted power of the ethanol solutions with WS_2 NPs to that without WS_2 NPs. Figure 1(e) shows the transmittance spectrum of WS_2 NP dispersion ranging from 400 to 900 nm (Andor SR500I), which is used to characterize the effective number of WS_2 layers in the SSPM experiment. There is no evident excitonic resonance feature in the transmission spectrum, which may be attributed to the decrease in the exciton binding energy due to the increase in the number of WS_2 layers [33].

The experimental setup for SSPM is schematically shown in Fig. 2(a). A femtosecond (fs) pulse laser (Coherent, Chameleon Ultra II, repetition frequency 80 MHz, pulse width 100 fs at 800 nm) propagates along the z axis and is loosely focused on the cuvette by a lens with a focal length of 200 mm. In the experiment, the incident power can be controlled using a set of neutral density (ND) filters. Then, diffraction patterns are recorded using a digital camera with a slow-motion function. Due to the SSPM effect, the transmitted light appeared as a set of conical shells, which form concentric rings on a 2D screen (Fig. 2). The outermost ring stripe is always brighter and wider than the inner ones. Interestingly, the initial concentric diffraction rings deform quickly [Fig. 2(b)]. The upper half of the ring pattern continuously collapses towards the center of the initial concentric rings and then enters a stable state. In contrast, the lower part distorts slightly. The evolution time from the generation of ring-shaped patterns to saturation of distortion phenomenon usually lasts from less than one second to several seconds, which relies on the impinging power.

3. RESULTS AND DISCUSSION

Generally, the SSPM phenomenon exhibits as a series of concentric diffraction rings on a projection screen when a high-intensity laser beam interacts with the nonlinear medium. The SSPM ring pattern is attributed to the laser-induced refractive index change Δn [34]. As the laser beam propagates along the z axis, the field E reorients the direction of WS_2 NPs in the

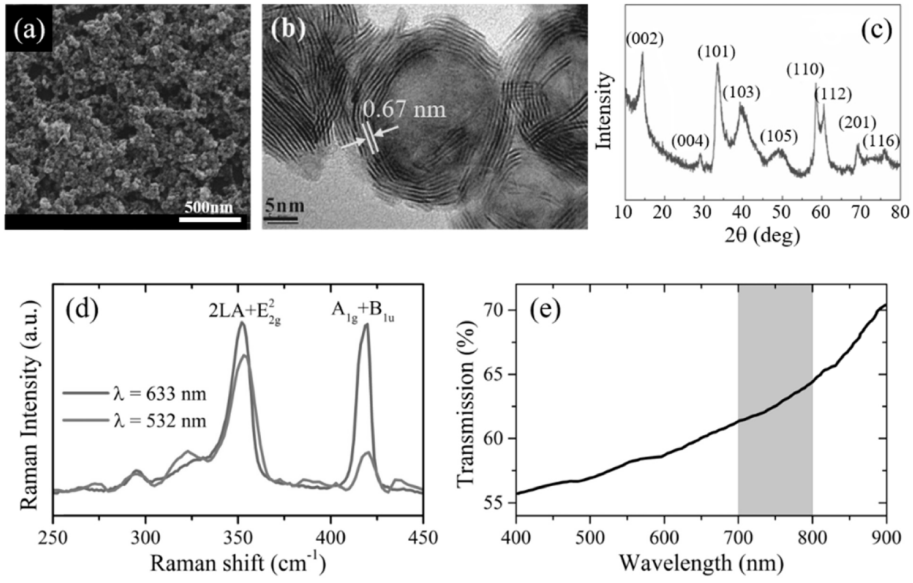

Fig. 1. Structure of IF-like WS_2 NPs and their optical response. (a) Scanning electron microscopy image, (b) high-resolution transmission electron microscopy image, and (c) X-ray diffraction pattern of the synthesized IF-like WS_2 NPs. (d) Raman spectra of the WS_2 dispersion excited by 633 and 532 nm lasers. (e) Transmittance of WS_2 NP dispersions. The interesting wavelength range is highlighted in the gray area.

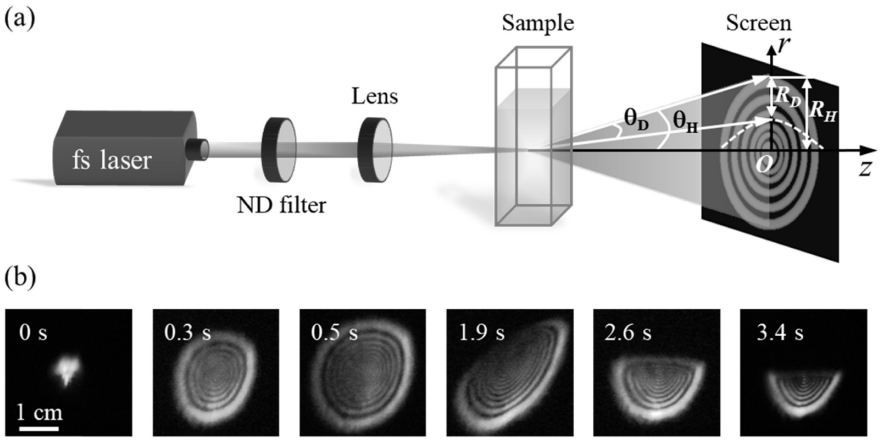

Fig. 2. (a) Schematic of the experimental setup and (b) evolution of the concentric ring-shaped diffraction patterns excited by a fs pulse laser at $\lambda = 800$ nm. The time capturing the diffraction patterns is inserted at the upper-left corner of each image.

normal plane. According to the Kerr effect, the refractive index of the suspension can be described by $n = n_0 + n_2 I$, where n_0 is the linear refractive index, n_2 is the nonlinear refractive index of WS_2 NPs, and I stands for the incident intensity of laser beam [1]. It should be noted that the self-focusing effect occurs when the beam enters into the Kerr media. The beam size rapidly converges into a minimum after a propagation length of less than one millimeter. Then, the beam propagates like a plane wave with a slightly increased diameter due to weak absorption and light scattering. Therefore, the self-focusing effect usually is not taken into account when measuring the nonlinear refractive index using SSPM [20].

After traversing the WS_2 dispersions of a thickness L, the incident light will gain an intensity-dependent phase [34]

$$\Delta\varphi(r) = \left(\frac{2\pi n_0}{\lambda}\right)\int_0^{L_{\text{eff}}} n_2 I(r,z)\mathrm{d}z, \tag{1}$$

where $I(r,z)$ is the intensity distribution of the focused laser beam, $r \in [0, +\infty)$ is the transverse coordinate in the beam, and the host solvent is ethanol with a refractive index of $n_0 = 1.36$. L_{eff} represents the effective interaction length contributing to the SSPM process, which can be calculated by $L_{\text{eff}} = \int_{L_1}^{L_2}(1 + z^2/z_0^2)^{-1}\mathrm{d}z = z_0 a\tan(z/z_0)|_{L_1}^{L_2}$, where $z_0 = \pi\omega_0^2/\lambda$, is defined by the waist width ω_0 and wavelength of the laser beam; $L = L_2 - L_1$ is the thickness of the quartz cuvette. In the experiment, $L = 10$ mm and $\omega_0 = 74.2$ μm at the front surface of the cuvette. For simplicity, the incident Gaussian laser with a cylindrical symmetry along the z axis will gain an additional phase shift $\Delta\varphi(r) = \Delta\varphi_0 \exp(-2r^2/\omega_0^2)$ after passing through the WS_2 dispersions. Here, $\Delta\varphi_0$ is the phase shift at the diffraction ring center, i.e., $r = 0$ [34]. By using Eq. (1), we obtain $\Delta\varphi_0 = 2\pi n_0 n_2 L_{\text{eff}} I/\lambda$ with $I(0,z) = 2I$ [35], which indicates that a larger intensity results in more phase shift. Since the temporal slot between pulses is 12.5 ns, all of the interference arises from the SSPM within each single pulse. Radiation fields from the area around two different points have the same wave vector and can cause interference. Maximum constructive or destructive interference is determined by $\Delta\varphi(r_1) - \Delta\varphi(r_2) = m\pi$, where m is an odd or even integer corresponding to dark or bright stripes, respectively. The total number of diffraction rings can be estimated as $N = [\Delta\varphi(0) - \Delta\varphi(\infty)]/2\pi = \Delta\varphi_0/2\pi$, which linearly increases as laser intensity increases [Fig. 3(a)]. In addition, at a given incident intensity, more rings pour out at longer wavelength irradiation.

The nonlinear refractive index can be expressed as [20,23]

$$n_2 = \frac{\lambda}{2n_0 L_{\text{eff}}}\frac{\mathrm{d}N}{\mathrm{d}I}. \tag{2}$$

The slope $S = \mathrm{d}N/\mathrm{d}I$ can be readily obtained by fitting intensity-dependent ring numbers, which increases as wavelength increases at a given intensity [Fig. 2(a)]. Moreover, the total third-order susceptibility can be obtained, $\chi^{(3)}_{\text{total}} = \frac{\lambda c n_0}{2.4\times10^4\times\pi^2 L_{\text{eff}}} S$ [20,23,36].

As introduced previously, third-order nonlinear susceptibility $\chi^{(3)}$ is of great significance for indicating nonlinear performance of the nonlinear materials. Here, the third-order nonlinear susceptibility of monolayer WS_2 NPs can be estimated using the counterpart of multiple layer structures with $\chi^{(3)}_{\text{total}} = N^2_{\text{eff}}\chi^{(3)}_{\text{monolayer}}$ [20,23], where N_{eff} represents the effective number of WS_2 layers in the NPs, and $\chi^{(3)}_{\text{monolayer}}$ represents the contribution of one layer WS_2 out of N_{eff} layers to the third-order susceptibility of WS_2 NPs. Therefore, $\chi^{(3)}_{\text{monolayer}}$ can be calculated with the following equation:

$$\chi^{(3)}_{\text{monolayer}} = \frac{n_0^2 n_2(\mathrm{cm}^2/\mathrm{W})}{0.0395 \times N^2_{\text{eff}}}. \tag{3}$$

The transmission of monolayer WS_2 is 99.3%–99.7% at the selected wavelength [23,37]. Therefore, according to the transmission measurement in Fig. 1(e), the effective layer number N_{eff} is estimated to be 48–140 at the wavelength ranging from 720 to 800 nm. Thus, the third-order susceptibility $\chi^{(3)}_{\text{monolayer}}$ for monolayer WS_2 is estimated to be in order of $\sim10^{-7}$ esu, which is two orders higher than the counterparts of popular 2D materials with planar features. Similar results are obtained when the solvent is replaced by methylbenzene. In addition, the n_2 of ethanol is ~9 orders smaller than the counterpart of the WS_2

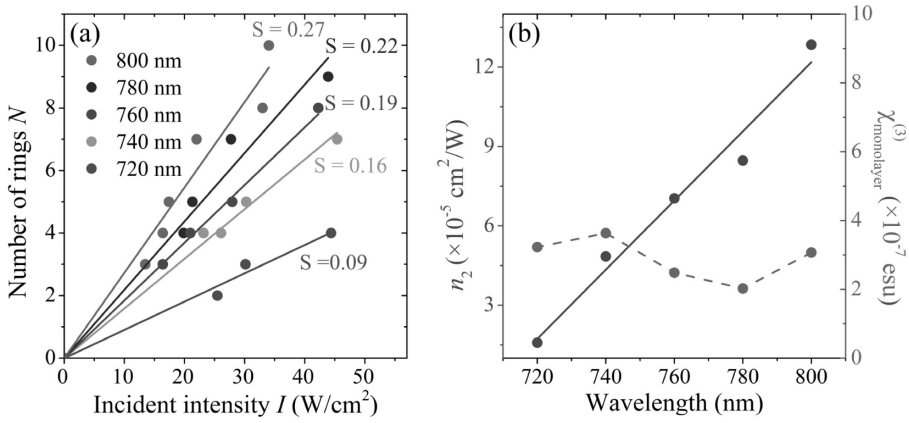

Fig. 3. (a) Dependence of the number of SSPM rings N on the laser intensity I at different wavelengths. (b) Dependence of nonlinear refractive index and third-order susceptibility of monolayer IF–WS_2 NPs on wavelength.

nanosheet [23], so the influence of the solvent on the final third-order nonlinearity can thus be excluded. As shown in Fig. 3(b), the third-order susceptibility $\chi^{(3)}_{\text{monolayer}}$ for monolayer WS_2 varies slightly around 720–800 nm. Both the nonlinear refractive index and third-order susceptibility $\chi^{(3)}_{\text{monolayer}}$ obtained by the SSPM experiment are listed for an explicit comparison (Table 1). Regarding the planar 2D WS_2, the introduced additional freedom by curved features plays an encouraging role in boosting up the nonlinear characteristics. On the other hand, compared with other 2D materials, such as black phosphorus (BP), IF-like WS_2 NPs with superior n_2 and $\chi^{(3)}_{\text{monolayer}}$ highlight a better idea of improving nonlinear optical properties.

Figure 2(b) briefly demonstrates the evolution of the diffraction pattern. The concentric rings pour out from the center. The diffraction pattern approaches the maximum geometric size within ~0.5 s (Fig. 4). Subsequently, both the horizontal and vertical diameters of the rings collapse and reach a steady state after ~2.8 s and ~4.5 s, respectively (Fig. 4). In contrast, the vertical diameter shrinks to half of the maximum one, while the horizontal diameter only compresses to 82% of the maximum one. The third-order nonlinearity is estimated when the number of rings becomes stable.

The distortion of diffraction rings is mainly attributed to the change of local material concentration induced by the non-axis-symmetrical thermal convection [43,44]. When the laser is incident upon the dispersions, the temperature surrounding the laser beam becomes asymmetrical, as the temperature gradient above the laser beam rises while it remains nearly stationary below the laser beam. As the non-axis-symmetrical thermal conduction increases [45], WS_2 NPs in the upper part of the dispersions are precipitated into the lower part, resulting in a smaller density of WS_2 NPs in the upper half of the dispersions, and then a reduced N_{eff}, naturally, with a reduced n_2. Therefore, the lower-half dispersions have a relatively stronger nonlinear optical response, leading to the vertical collapse of the SSPM diffraction rings. Notably, the vertical deformation of SSPM rings is of great significance for the study of the photorefractive index change of IF-like WS_2 NPs.

The maximum value of the vertical radius of the outermost ring and its half-cone angle are denoted by R_H and θ_H, respectively. The half-cone angle can be written as $\theta_H = \lambda/2\pi(\mathrm{d}\Delta\varphi/\mathrm{d}r)_{\max}$, which can be further simplified, for a Gaussian beam, to be $\theta_H \approx n_2 IC$, where $C = [-(8IrL_{\text{eff}}/\omega_0^2) \times \exp(2r^2/\omega_0^2)]_{\max}$ with $r \in [0, +\infty)$ being a constant. The distortion angle can be expressed as $\theta_D \approx \Delta n_2 IC$, where Δn_2 is the nonlinear refractive index change caused by intensity variation. Eventually, the change ratio of the nonlinear refractive index can be calculated [39,43].

An increased incident intensity induces a more obvious distortion. Figure 5 exhibits the relationship between incident intensity and $\Delta n_2/n_2$ at different wavelengths. To a certain extent, the linear regulation of the refractive index change of the material can be achieved by adjusting the intensity of the applied optical field. Nevertheless, the distortion ratio

Table 1. n_2 and $\chi^{(3)}_{\text{monolayer}}$ for Different 2D Materials Obtained by SSPM

2D Materials	n_2 (cm²/W)	$\chi^{(3)}_{\text{monolayer}}$ (esu)	Laser Wavelength (nm)	References
Graphene	2.5×10^{-5}	10^{-7}	532, CW	[20]
$MoS_2/WS_2/MoSe_2$	$\sim 10^{-7}$	10^{-9}	488, CW	[23]
BP	$\sim 10^{-5}$	$\sim 10^{-8}$	350–1160, pulse	[38]
SnS	$\sim 10^{-5}$	$\sim 10^{-10}$	532/633, CW	[39]
Antimonene	$\sim 10^{-5}$	$\sim 10^{-8}$	405/785/1064, CW	[40]
$Ti_3C_2T_x$	$\sim 10^{-4}$	$\sim 10^{-7}$	457/532/671, CW	[41]
Te	$\sim 10^{-5}$	/	457/532/671, CW	[42]
WS_2 NPs	$\sim 10^{-5}$	$\sim 10^{-7}$	720–800, pulse	This work

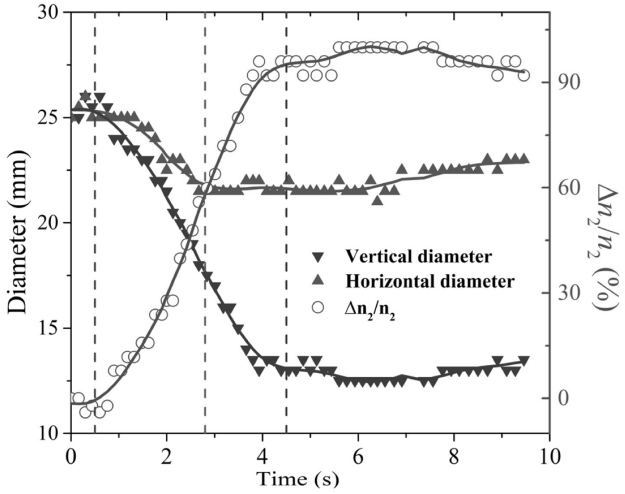

Fig. 4. Evolution of the diameter of the outermost SSPM ring along the vertical and horizontal directions and $\Delta n_2/n_2$ at $\lambda = 800$ nm.

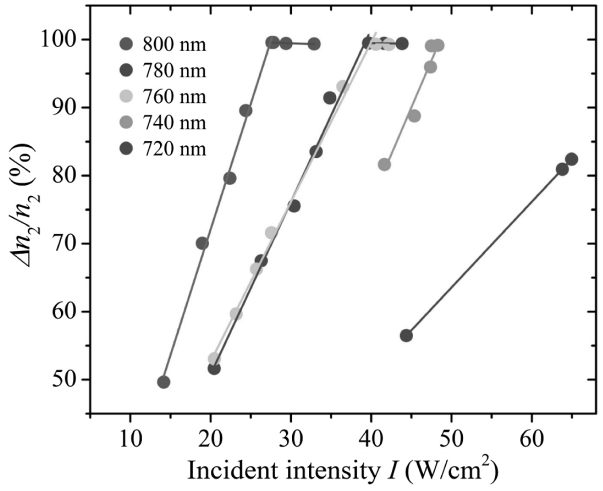

Fig. 5. Dependence of $\Delta n_2/n_2$ on the incident intensity at different wavelengths.

cannot be infinitely large due to the limitation $\theta_D < \theta_H$. When the incident intensity reaches the wavelength-dependent threshold of approximately 30–40 W/cm^2, the distortion ratio is prone to saturation (Fig. 5). Even so, the Kerr effect itself is not saturated. Since the saturation of the distortion phenomenon is mainly influenced by the non-axis-symmetrical thermal convection, a vertically rising temperature gradient causes WS_2 NPs to continuously sink below the laser beam. After a period of thermal convection, when the density of WS_2 NPs above the laser beam is infinitely close to zero, the upper part of the diffraction rings gradually approaches complete collapse.

As shown in Table 1, only the third-order nonlinear performance of $Ti_3C_2T_x$ MXene exceeds the counterparts of the proposed WS_2 NPs. However, the underlying mechanism here is different from those observed in $Ti_3C_2T_x$ MXene with a narrow direct bandgap [41]. Because of the multiple layers in WS_2 NPs, no photoluminescence (PL) emission is observed in our experiment [46,47]. Therefore, no interband transition occurs. The electrons are delocalized by the polarized incident field. The nonlinear refractive index can be estimated by $\chi^{(3)} \approx Ne^4/\varepsilon_0 m^3 \omega_{e0}^6 d^2$, where e is the element charge, ε_0 is the vacuum permittivity, N is the density of electrons of the material, ω_{e0} is the oscillation frequency of electrons, $\omega_{e0} = me^4/32\pi^2\varepsilon_0^2\hbar^3$, d is the lattice constant, and m is the effective mass of the conduction electron [1]. If d is identified with the Bohr radius $a_0 = 4\pi\varepsilon_0\hbar^2/me^4$, we obtain that $\chi^{(3)} \propto m^{-7}$. Due to the distortion and curved features in WS_2 NPs, the effective mass of electrons in IF-like WS_2 NPs is speculated to reduce in comparison with the counterparts in planar 2D materials [25]. Therefore, the reduced effective mass of electrons will contribute to a portion of the enhancement in n_2 and $\chi^{(3)}$.

The mechanism of the SSPM phenomenon in WS_2 NPs dispersion is essentially an appearance of intensity-dependent change in the refractive index. In principle, the thermal effect can only play a crucial role when the pulse duration is longer than tens of picoseconds. Therefore, the thermal contribution plays a non-dominated role in n_2 and $\chi^{(3)}$ enhancement under the illumination of the fs pulse source. Nevertheless, its contribution may be comparable to the contribution of the reduced effective mass of electrons. The electrons and holes generated by photoexcitation will drift in directions that are antiparallel and parallel to the electric field, respectively, resulting in polarized WS_2 NPs. Initially, an arbitrary angle related to the interaction energy exists between the direction of the WS_2 NPs polarization and the laser-induced electric field. As interaction energy is minimized, WS_2 NPs are reoriented and aligned. The isotropy of the carriers in each particle appears as a kind of coherence that contributes to the macroscopic SSPM phenomenon. While it has another explanation, the gap-dependent SSPM can be regarded as a purely coherent third-order nonlinear optical process, which is generated from the nonlocal ac electron coherence within the sample [35]. Since each WS_2 NP is mimicked as a separated domain containing multiform carriers, anisotropic domains are reoriented to alignment attributed to the torque produced by interior electron coherence influenced by an external electromagnetic field and finally polarized. The dielectric polarization caused by the electron coherence effect can be regarded as the collective behavior of a large number of electrons within the sample. Similarly, the polarization induced by the drift of photoexcited carriers (holes) can also be considered as a collective behavior of carriers.

Recently, it was demonstrated that second-harmonic generation can be actively controlled via the generation of photocarriers in monolayer MoS_2 using ultrashort pulses, which enables a promising time-resolved approach to characterize the second-order nonlinear response [48]. A similar approach is also promising for extension into unveiling the detailed physical mechanism of the enhanced third-order nonlinear properties of WS_2 NPs.

4. CONCLUSION

In conclusion, a novel type of IF-like WS_2 NPs is successfully synthesized using the hard template method with a diameter of 26.5 nm. By characterizing the nonlinear refractive index n_2 and third-order susceptibility $\chi^{(3)}$ using the SSPM method

with a visible fs pulse laser, we obtain $n_2 \sim 10^{-5}$ cm^2/W and $\chi^{(3)} \sim 10^{-7}$ esu, which are orders stronger than the counterparts of planar 2D materials. In addition, the enhanced third-order nonlinear response can be controlled flexibly by varying the excitation wavelength and incident intensity, which is beneficial for all-optical devices. Therefore, IF-like 2D materials will enrich the optical materials with superior efficiencies, and are endowed with promising potentials in photonic integration applications.

Funding. Fundamental Research Funds for the Central Universities (Z201805196); Natural Science Foundation of Shaanxi Province (2018JM6001); Young Talent Recruiting Plans of Xi'an Jiaotong University.

Disclosures. The authors declare no conflicts of interest.

†These authors contributed equally to this work.

REFERENCES

1. R. Boyd, *Nonlinear Optics*, 3rd ed. (Elsevier, 2008).
2. S. Sakabe, C. Lienau, and R. Grunwald, *Progress in Nonlinear Nano-Optics* (Springer, 2015).
3. M. Lapine, I. V. Shadrivov, and Y. S. Kivshar, "Colloquium: nonlinear metamaterials," Rev. Mod. Phys. **86**, 1093–1123 (2014).
4. A. Autere, H. Jussila, Y. Dai, Y. Wang, H. Lipsanen, and Z. Sun, "Nonlinear optics with 2D layered materials," Adv. Mater. **30**, 1705963 (2018).
5. T. Ozawa, H. M. Price, A. Amo, N. Goldman, M. Hafezi, L. Lu, M. C. Rechtsman, D. Schuster, J. Simon, and O. Zilberberg, "Topological photonics," Rev. Mod. Phys. **91**, 015006 (2019).
6. A. Vakil and N. Engheta, "Transformation optics using graphene," Science **332**, 1291–1294 (2011).
7. H. Lin, B. C. P. Sturmberg, K.-T. Lin, Y. Yang, X. Zheng, T. K. Chong, C. M. de Sterke, and B. Jia, "A 90-nm-thick graphene metamaterial for strong and extremely broadband absorption of unpolarized light," Nat. Photonics **13**, 270–276 (2019).
8. G. Hu, X. Hong, K. Wang, J. Wu, H.-X. Xu, W. Zhao, W. Liu, S. Zhang, F. Garcia-Vidal, B. Wang, P. Lu, and C.-W. Qiu, "Coherent steering of nonlinear chiral valley photons with a synthetic Au-WS_2 metasurface," Nat. Photonics **13**, 467–472 (2019).
9. D. J. K. S. Novoselov, F. Schedin, T. J. Booth, V. V. Khotkevich, S. V. Morozov, and A. K. Geim, "Two-dimensional atomic crystals," Proc. Natl. Acad. Sci. USA **102**, 10451–10453 (2005).
10. A. K. Geim and I. V. Grigorieva, "Van der Waals heterostructures," Nature **499**, 419–425 (2013).
11. Y. S. Ang, S. Sultan, and C. Zhang, "Nonlinear optical spectrum of bilayer graphene in the terahertz regime," Appl. Phys. Lett. **97**, 243110 (2010).
12. A. Wright, X. Xu, J. Cao, and C. Zhang, "Strong nonlinear optical response of graphene in the terahertz regime," Appl. Phys. Lett. **95**, 072101 (2009).
13. F. Xia, H. Wang, D. Xiao, M. Dubey, and A. Ramasubramaniam, "Two-dimensional material nanophotonics," Nat. Photonics **8**, 899–904 (2014).
14. D. N. Basov, M. M. Fogler, and F. J. Garcia de Abajo, "Polaritons in van der Waals materials," Science **354**, aag1992 (2016).
15. Y. Xu, Y. S. Ang, L. Wu, and L. K. Ang, "High sensitivity surface plasmon resonance sensor based on two-dimensional MXene and transition metal dichalcogenide: a theoretical study," Nanomaterials **9**, 165 (2019).
16. M. Taghinejad and W. Cai, "All-optical control of light in micro- and nanophotonics," ACS Photon. **6**, 1082–1093 (2019).
17. M. Sheik-Bahae, A. A. Said, and E. W. Van Stryland, "High-sensitivity, single-beam n_2 measurements," Opt. Lett. **14**, 955–957 (1989).
18. X. Jiang, S. Liu, W. Liang, S. Luo, Z. He, Y. Ge, H. Wang, R. Cao, F. Zhang, Q. Wen, J. Li, Q. Bao, D. Fan, and H. Zhang, "Broadband nonlinear photonics in few-layer MXene $Ti_3C_2T_x$ (T = F, O, or OH)," Laser Photon. Rev. **12**, 1700229 (2018).
19. Z. Zhang and P. L. Voss, "Full-band quantum-dynamical theory of saturation and four-wave mixing in graphene," Opt. Lett. **36**, 4569–4571 (2011).
20. R. Wu, Y. Zhang, S. Yan, F. Bian, W. Wang, X. Bai, X. Lu, J. Zhao, and E. Wang, "Purely coherent nonlinear optical response in solution dispersions of graphene sheets," Nano Lett. **11**, 5159–5164 (2011).
21. J. Zhang, M. Ye, S. Bhandari, A. K. M. Muqri, F. Long, S. Bigham, Y. K. Yap, and J. Y. Suh, "Enhanced second and third harmonic generations of vertical and planar spiral MoS_2 nanosheets," Nanotechnology **28**, 295301 (2017).
22. J. Sun, Y.-J. Gu, D. Y. Lei, S. P. Lau, W.-T. Wong, K.-Y. Wong, and H. L.-W. Chan, "Mechanistic understanding of excitation-correlated nonlinear optical properties in MoS_2 nanosheets and nanodots: the role of exciton resonance," ACS Photon. **3**, 2434–2444 (2016).
23. G. Wang, S. Zhang, X. Zhang, L. Zhang, Y. Cheng, D. Fox, H. Zhang, J. N. Coleman, W. J. Blau, and J. Wang, "Tunable nonlinear refractive index of two-dimensional MoS_2, WS_2, and $MoSe_2$ nanosheet dispersions [Invited]," Photon. Res. **3**, A51–A55 (2015).
24. J. Song, L. Zhang, Y. Xue, Q. Y. S. Wu, F. Xia, C. Zhang, Y.-L. Zhong, Y. Zhang, J. Teng, and M. Premaratne, "Efficient excitation of multiple plasmonic modes on three-dimensional graphene: an unexplored dimension," ACS Photon. **3**, 1986–1992 (2016).
25. G. L. Frey, S. Elani, M. Homyonfer, Y. Feldman, and R. Tenne, "Optical-absorption spectra of inorganic fullerene-like MS_2 (M=Mo, W)," Phys. Rev. B **57**, 6666–6671 (1998).
26. M. Krause, M. Virsek, M. Remskar, N. Salacan, N. Fleischer, L. Chen, P. Hatto, A. Kolitsch, and W. Moller, "Diameter and morphology dependent Raman signatures of WS_2 nanostructures," Chemphyschem **10**, 2221–2225 (2009).
27. Y. B. L. Rapoport, Y. Feldman, M. Homyonfer, S. R. Cohen, and R. Tenne, "Hollow nanoparticles of WS_2 as potential solid-state lubricants," Nature **387**, 791–793 (1997).
28. L. Rapoport, N. Fleischer, and R. Tenne, "Applications of WS_2 (MoS_2) inorganic nanotubes and fullerene-like nanoparticles for solid lubrication and for structural nanocomposites," J. Mater. Chem. **15**, 1782–1788 (2005).
29. R. Hao, L. Zhang, L. Zhang, H. You, J. Fan, and J. Fang, "Curved 2D WS_2 nanostructures: nanocasting and silent phonon mode," Nanoscale **12**, 9038–9047 (2020).
30. M. Staiger, P. Rafailov, K. Gartsman, H. Telg, M. Krause, G. Radovsky, A. Zak, and C. Thomsen, "Excitonic resonances in WS_2 nanotubes," Phys. Rev. B **86**, 165423 (2012).
31. J. Verble and T. Wieting, "Lattice mode degeneracy in MoS_2 and other layer compounds," Phys. Rev. Lett. **25**, 362–365 (1970).
32. X. Zhang, X.-F. Qiao, W. Shi, J.-B. Wu, D.-S. Jiang, and P.-H. Tan, "Phonon and Raman scattering of two-dimensional transition metal dichalcogenides from monolayer, multilayer to bulk material," Chem. Soc. Rev. **44**, 2757–2785 (2015).
33. G. D. Scholes and G. Rumbles, "Excitons in nanoscale system," Nat. Mater. **5**, 683–696 (2006).
34. S. Durbin, S. Arakelian, and Y. Shen, "Laser-induced diffraction rings from a nematic-liquid-crystal film," Opt. Lett. **6**, 411–413 (1981).
35. Y. Wu, Q. Wu, F. Sun, C. Cheng, S. Meng, and J. Zhao, "Emergence of electron coherence and two-color all-optical switching in MoS_2 based on spatial self-phase modulation," Proc. Natl. Acad. Sci. USA **112**, 11800–11805 (2015).
36. B. Shi, L. Miao, Q. Wang, J. Du, P. Tang, J. Liu, C. Zhao, and S. Wen, "Broadband ultrafast spatial self-phase modulation for topological insulator Bi_2Te_3 dispersions," Appl. Phys. Lett. **107**, 151101 (2015).
37. M. Bernardi, M. Palummo, and J. C. Grossman, "Extraordinary sunlight absorption and one nanometer thick photovoltaics using two-dimensional monolayer materials," Nano Lett. **13**, 3664–3670 (2013).
38. J. Zhang, X. Yu, W. Han, B. Lv, X. Li, S. Xiao, Y. Gao, and J. He, "Broadband spatial self-phase modulation of black phosphorous," Opt. Lett. **41**, 1704–1707 (2016).
39. L. Wu, Z. Xie, L. Lu, J. Zhao, Y. Wang, X. Jiang, Y. Ge, F. Zhang, S. Lu, Z. Guo, J. Liu, Y. Xiang, S. Xu, J. Li, D. Fan, and H. Zhang,

"Few-layer tin sulfide: a promising black-phosphorus-analogue 2D material with exceptionally large nonlinear optical response, high stability, and applications in all-optical switching and wavelength conversion," Adv. Opt. Mater. **6**, 1700985 (2018).
40. G. Wang, S. Higgins, K. Wang, D. Bennett, N. Milosavljevic, J. J. Magan, S. Zhang, X. Zhang, J. Wang, and W. J. Blau, "Intensity-dependent nonlinear refraction of antimonene dispersions in the visible and near-infrared region," Appl. Opt. **57**, E147–E153 (2018).
41. L. Wu, X. Jiang, J. Zhao, W. Liang, Z. Li, W. Huang, Z. Lin, Y. Wang, F. Zhang, S. Lu, Y. Xiang, S. Xu, J. Li, and H. Zhang, "MXene-based nonlinear optical information converter for all-optical modulator and switcher," Laser Photon. Rev. **12**, 1800215 (2018).
42. L. Wu, W. Huang, Y. Wang, J. Zhao, D. Ma, Y. Xiang, J. Li, J. S. Ponraj, S. C. Dhanabalan, and H. Zhang, "2D tellurium based high-performance all-optical nonlinear photonic devices," Adv. Funct. Mater. **29**, 1806346 (2019).
43. G. Wang, S. Zhang, F. A. Umran, X. Cheng, N. Dong, D. Coghlan, Y. Cheng, L. Zhang, W. J. Blau, and J. Wang, "Tunable effective nonlinear refractive index of graphene dispersions during the distortion of spatial self-phase modulation," Appl. Phys. Lett. **104**, 141909 (2014).
44. C. M. Vest and M. Lawson, "Onset of convection near a suddenly heated horizontal wire," Int. J. Heat Mass Transfer **15**, 1281–1283 (1972).
45. W. C. W. Ji, S. Lim, J. Lin, and Z. Guo, "Gravitation-dependent, thermally-induced self-diffraction in carbon nanotube solutions," Opt. Express **14**, 8958–8966 (2006).
46. A. Splendiani, L. Sun, Y. Zhang, T. Li, J. Kim, C. Y. Chim, G. Galli, and F. Wang, "Emerging photoluminescence in monolayer MoS_2," Nano Lett. **10**, 1271–1275 (2010).
47. K. F. Mak, C. Lee, J. Hone, J. Shan, and T. F. Heinz, "Atomically thin MoS_2: a new direct-gap semiconductor," Phys. Rev. Lett. **105**, 136805 (2010).
48. M. Taghinejad, Z. Xu, H. Wang, H. Taghinejad, K.-T. Lee, S. P. Rodrigues, A. Adibi, X. Qian, T. Lian, and W. Cai, "Photocarrier-induced active control of second-order optical nonlinearity in monolayer MoS_2," Small **16**, 1906347 (2020).